# USE OF CO-POLAR CORRELATION COEFFICIENT FOR PROBING PRECIPITATION AT NEARLY VERTICAL INCIDENCE

**D.S. Zrnic**[1], N. **Balakrishnan**[2], A. Ryzhkov[3], and
NOAA/Environmental Research Laboratories
National Severe Storms Laboratory
Norman OK, 73069

**S.L. Durden**
Jet Propulsion Laboratory
California Institute of Technology
Pasadena, CA91109

ABSTRACT

We present observations of the co-polar correlation coefficient $|\rho_{hv}(0)|$ made with ground based and airborne weather radars at nearly vertical incidence. A sharp decrease of $|\rho_{hv}(0)|$ occurs at the bright band bottom and is attributed to a varying mixture ofhydrometeors with diverse shape, size, and thermodynamic phase. The largest contribution to **decorrelation** seems to come from wet aggregates; this is substantiated by consideration of two simple models. One consists 'of randomly oriented wet prolate spheroids and the other considers an ensemble of distorted spheres. Prelates with axis ratios of 3 or distorted spheres with rms roughness equal to **15% of** the diameter decrease the correlation to 0.8 at S-band. At Ku-band and for the size range encountered in the bright band the decrease is a function of equivalent diameter because scattering is in the **Mie** regime. .

---

'National Severe Storms Laboratory, 1313 Halley Circle, Norman, OK 73069

[2]**Visiting** scientist at the Cooperative Institute for **Mesoscale** Meteorological Studies **(CIMMS)** from Indian Institute of Science, **Bangalore,** India.

[3]**National** Research Council senior postdoctoral fellow, on leave from the Main Geophysical Observatory, St. Petersburg, Russia.

$|\rho_{hv}(0)|$ measurement at 13.8 GHz and from the aircraft are the first ever. Also differential phase and differential reflectivity at a $10^{\circ}$ off nadir are the first of its kind. These last two variables showed a distinct signature in the bright band. This is significant because it might lead to "applications on airborne or space-borne platforms.

## 1.0 INTRODUCTION

There have been few polarimetric measurements at vertical incidence from ground based radars and very few at any incidence from aircraft. Notable are observations at nadir by Kumagai et al, [1] who have shown that the linear depolarization ratio (LDR) can be used to determine the phase state of hydrometers and to identify the melting layer. Observations of the correlation coefficient $|\rho_{hv}(0)|$ between linear co-polar components were made at vertical incidence with ground based radars [2]. These measurements showed that $|\rho_{hv}(0)|$ . can also be used to identify the melting layer. Other polarimetric variables such as differential reflectivity $Z_{DR}$ and differential phase $\phi_{DP}$ (due to propagation and backscatter) are related to average shapeof hydrometeors andare most effective forhydrometeor identification if measured at horizontal incidence [3]. Consequently, these variables have not been studied for incidence near vertical.

Here, we describe and interpret ground-based and airborne polarimetric radar observations of precipitation at and near vertical incidence. Included is an example of $Z_{DR}$ and $\phi_{DP}$ obtained at 10° off nadir which demonstrates that meaningful interpretations of these variables might be possible at relatively small nadir angles to which space-borne platforms are constrained.

Observations are from two radar systems. NSSL's Cimarron radar (Table 1) provides $|\rho_{hv}(0)|$ in real time and at 768 range locations [4]. The radar transmits an alternating sequence of H and V polarizations, and a procedure suggested by Balakrishnan and Zrnic [5] is used to obtain $|\rho_{hv}(0)|$. TheNASA/JPL airborne rain mapping radar (ARMAR) operates (Table 2) in a variety of single and dual-polarization modes; its antenna is pointing downward and can scan accross track. The data presented here were obtained using an alternating H and V sequence and were processed after the fact to produce the correlation, the differential reflectivity, and the differential phase.

## 2.0 CORRELATION COEFFICIENT

The 'correlation coefficient is defined by

$$\rho_{hv}(0) = \langle s_{vv} s^*_{hh} \rangle / \left[ \langle |s_{hh}|^2 \rangle^{1/2} \langle |s_{vv}|^2 \rangle^{1/2} \right] \quad (1)$$

Here $s_{ij}$ is the element of the backscatter matrix of a hydrometer. The first subscript in $s_{ij}$ refers to the polarization of the backscattered field (h or v) and the second to the polarization of the incident. field. In $\rho_{hv}$ the subscript h or v is used to denote the polarization of the co-polar transmitted and received waves. The brackets are expectations expressed in terms of the distribution of the hydrometeor's properties (i.e. equivalent volume diameter, shape, canting angle etc.).

There are several meteorological factors that influence $|\rho_{hv}(0)|$. These are related to apparent shape, size, and backscatter differential phase, all of which often occur simultaneously in nature. Under ideal conditions (without

noise and/or artifacts) the mean correlation coefficient from pure rain at vertical incidence would be larger than 0.99 [6]. This is because, at vertical incidence, shape variation with size is not apparent and the decrease in correlation would be due to secondary effects such as drop oscillations, coalescence, and breakup etc. Fairly 1 arge values of $|\rho_{hv}(0)|$ are also expected from most frozen precipitation, but a decrease could occur in the presence of hail, large wet aggregates and mixed phase precipitation.

Decorrelation occurs if the two orthogonal backscattered fields do not vary in unison, i.e. there must be a change of the net effective backscattering properties at horizontal and vertical polarizations in the resolution volume. This can occur if the changes of the two fields for various particles in the ensemble are not proportional to each other and there is reorientation or motion and/or replenishment of the particles during dwell time. The fields also change differently if there is a variation of backscatter differential phase from hydrometer to hydrometer, Such variations can occur i f scattering is in the Mie regime; Zrnic et al. [7] show evidence of significant backscatter differential phase at the bottom of the melting 1 ayer (observed with a horizontally pointing beam) and attribute a portion of the decrease in $|\rho_{hv}(0)|$ to this effect.

There have been few measurements of the correlation coefficient at vertical incidence [2] and the first ones from an airborne platform are presented here. Observations with a horizontally pointing beam show that the distribution of shapes (i.e., eccentricity of oblate spheroids due to dependence on size) decreases the correlation, for example Balakrishnan and Zrnic [5] report a mean value of 0.98, whereas Illingworth and Caylor [8] measured, with a high resolution (beamwidth 0.25 deg) radar, values between 0.985 and 0.995. The

physical reason for this dependence is that changes in reflectivities at horizontal and vertical polarization are not equal for the same increment in size/volume of hydrometers.

## 3.0 SCATTERING MODELS

For computing scattering coefficients, hydrometeors are often approximated with prolate or oblate spheroids. At a 10 cm wavelength, wet hydrometers smaller than 1 cm are in the Rayleigh scattering regime for which the Rayleigh-Guns theory can be used to compute the backscatter amplitudes and hence the correlation [3]. At a 2 cm wavelength these same hydrometers might be in the Mie scattering regime and the Rayleigh approximation may not be valid. Another drawback of the Rayleigh approximation is that 'the computed $|\rho_{hv}(0)|$ is independent of the size of the spheroids. Hence, in this paper, more accurate but computationally intensive calculations based on the T-matrix method [9] are performed for the 13.8 GHz frequency.

The variety of hydrometer shapes in the melting layer is large, but for computing $|\rho_{hv}(0)|$ we use prolate spheroids and for computing $Z_{DR}$ and $\phi_{DP}$ we use oblate spheroids (the reason for this choice will be explained shortly). In this manner, qualitative if not quantitative description of bulk hydrometer properties can be obtained.

Prolate spheroids: Randomly oriented prolate spheroids in the plane of polarization are a reasonable model for elongated hydrometeors. This model can also be used to calculate the correlation coefficient of irregular hydrometeors. From the value of the correlation coefficient it is not possible to deduce if backscattering hydrometeors are elongated but randomly oriented or if the shapes are rugged (symmetric or irregular). T-matrix computations were made forprol ate

spheroids with axis ratios of 2 and 3, and dielectric constant of water. Prelates were assumed to have a uniformly random orientation in the plane of polarization and in Fig. 1 are the values of $|\rho_{hv}(0)|$ as a function of equivolume diameters. It can be seen that $|\rho_{hv}(0)|$ is smaller for larger axis ratios.

One of the measurements from the airborne radar (See 4,2) was made at 10° off nadir as depicted in Fig. 2; differential reflectivity and backscatter differential phase produced distinct signatures in the melting layer. Our model of randomly oriented prolate spheroids is adequate for particles in the melting layer. Modeling random orientation of these scatterers requires a large amount of computations if scattering is non Rayleigh and is unavoidable for simulating $|\rho_{hv}(0)|$. Nevertheless, differential reflectivity and backscatter differential phase $\delta$ (i.e. the contribution to $\phi_{DP}$ by backscattering hydrometeors) depend on the mean orientation with respect to the hand v vectors whereas $|\rho_{hv}(0)|$ depends on the distribution of orientations. Therefore it is always possible to find oblate spheroids which will give the same $\phi_{DP}$ or $\delta$ as would a random distribution of prolate spheroids.

Oblate spheroids: We modeled observation at an incidence angle of 10° because this was the angle at which a radial of data was obtained. We considered two spatial configurations, in one the vertical E field is co planar with the symmetry axis of the hydrometer and in the other the drop is canted by 20°. The latter was the actual geometry (Fig. 2). The $Z_{DR}$ and $\delta$ values for axis ratios of0.3 and 0.4 and a canting angle of20° are plotted in Fig. 3). Note that more oblate scatterers (a/b = 0.3) produce larger $Z_{DR}$ and larger deviation of $\delta$ from zero than less oblate scatterers (a/b = 0.4). This trend seems to extrapolate to smaller axis ratios (a/b < 0.3) but, because of numerical instabilities, it could only be partly verified with the T matrix computations.

## 4.0 MEASUREMENTS

In this section, we present the measurements with a vertically-pointing ground based radar and a nadir pointing airborne radar.

### 4.1 OBSERVATIONS WITH THE GROUND BASED RADAR

Sample measurements in a precipitation event were collected using NSSL's 10 cm wavelength polarimetric radar (Cimarron) located 40 km northwest of Norman OK. Values of $|\rho_{hv}(0)|$, reflectivity factor Z, Doppler velocity v, and spectrum width $\sigma_v$, obtained from a stratiform region of a mesoscale convective system of 5 June 1992 are presented in Fig. 4. The profile of Z depicts a typical bright band [10]; a layer of reflectivity above 30 dBZ is seen between 3 and 3.6 km, this is just under the zero degree isotherm which onthis day was at3.6 km. The dip in correlation occurs at the bottom of the reflectivity layer (3 km). Similar dips of the correlation coefficient at the bottom of the melting layer were previously observed with the antenna beam at low elevation angles; these were attributed to the variety of sizes and shapes and rapid changes of the differential phase shift upon scattering [7], [8]. Just before collapsing into drops, large aggregates are very irregular and soaked with water, moreover, at that time there is also a substantial amount of drops coexisting in the resolution volume; both these effects tend to decrease the correlation.

The enlarged profiles in Fig. 4e illustrate the variations in $|\rho_{hv}(0)|$, Z and v through the melting layer. The change of the velocity from -1 to -7 m S-l (Fig. 4c) occurs between 3.45 and 2.85 km, Over the same height interval there is an increase of the spectrum width (from 1 to 2.5 m S-l in Fig. 4d). Obviously

the relative amounts of liquid and ice precipitation change within this interval from predominantly ice to rain, that is also where the location of the $|\rho_{hv}(0)|$ dip (Fig. 4e) is centered. There the combined effect of irregular, high-reflective wet aggregates and a highly diverse particle population at various stages of melting is strongest. At the first range location below the dip the correlation coefficient has not yet fully recovered indicating that large aggregates may be present, in addition to drops, within the resolution volume. Note that a smaller number of large aggregates or irregular drops (with ice cores) are sufficient to reduce the correlation even if the number of spherical small drops is high because the contributions to the correlation coefficient are weighted by the scatterer's cross section.

Examination of $|\rho_{hv}(0)|$ at 1000 consecutive radials (Fig. 5) indicates little change with time. The return to higher values is very sharp just below the melting layer (2.75 km) and between 3.1 and3.4 kmthere is some evidence of advection and evolution.

One of the contributing causes to the decrease of correlation at horizontal incidence is the rapid variation of differential phase shift upon scattering with change in aggregate dimensions. It is not necessary to invoke this Mie effect to explain the decrease of $|\rho_{hv}(0)|$ at vertical incidence. Comparison with simple models (Rayleigh-Gans scattering, Fig. 8.27 in [3]) suggests that randomly oriented wet prolate spheroids with an axis ratio of about 4 would produce a correlation coefficient of less than 0.8, Similar value is obtained from wet distorted spheres with an rmsdistortion to diameter ratio of 0.15 (Fig. 8.28 in [3]). From this it can be construed that hydrometers have at least this much variation in shape at the bottom of the melting layer.

## 4.2 OBSERVATIONS WITH AIRBORNE RADAR

Identification of the melting layer from airborne platforms s important to the measurement of precipitation from space. Kumagai et al. [1] used a polarimetric rain radar to measure Linear Depolarization Ratio (LDR) from the NASA DC-8 aircraft. Their preliminary measurements indicate that it impossible to use LDR in distinguishing among various types of hydrometers even at near-nadir incidence. They also observed that the cross polarization signal (15 to 30 dB lower than the co-polar signal) is often smaller than the receiver noise. It can be expected that the measurement of $|\rho_{hv}(0)|$ would be less contaminated by noise since it is the correlation between two strong co-polar returns; but, $|\rho_{hv}(0)|$ is affected by the fl actuations in the aircraft motion. In order to examine this and also explore the utility of $|\rho_{hv}(0)|$ measurement from airborne platforms, sample data from the NASA/JPL ARMAR system are analyzed and the results are presented in this section.

On May 25, 1992, data was collected from convective cells over the tropical Pacific. 600 radials of time series data (i.e., in phase and quadrature components), each with 512 range gates spaced 30 m apart were available for analysis. The vertical profile of Z, $|\rho_{hv}(0)|$, v, and $\sigma_v$ are shown in Fig. 6. As expected at vertical incidence both $Z_{DR}$ and $\phi_{DP}$ (not shown) had no discernible features to aid in the identification of hydrometeors. The reflectivity factor increases from about 20 dBZ at 6 kmto its peak of45 dBZ at 3.7 km; the profile is similar to that shown in Fig. 4. No measurement of zero degree isotherm was available for this day; but on 21 May 1992, the zero degree isotherm was measured to be at 4.7 km, and this is consistent with the Z profile in Fig. 6a.

The $|\rho_{hv}(0)|$ in Fig. 6b was computed using forward and inverse Fourier

transform to interpolate the time series data (Appendix). The minima of $|\rho_{hv}(0)|$ occur at 4.2 km and 2.7 km. Furthermore, the minimum of $|\rho_{hv}(0)|$ for the aircraft data is lower (0.6) compared to that measured through the melting layer from thegroundbased S band radar (0.8, Figs. 4 and 5). This is to be expected, considering that the airborne radar's operating frequency is 13.8 GHz; the Mie effects that cause resonances in scattering amplitudes and phases become effective for smaller sizes, contributing to an increased decorrelation. The first minimum at4.2kmis just below the zero degree isotherm and is most likely caused by the variety In shape and sizes of the hydrometers that are generated by the melting process. From the 0.6 value and Fig. 1 we speculate that the equivalent diameters of contributing hydrometers could be in the range 6 to 8 mm and axis ratios of near 3. The width of the $|\rho_{hv}(0)|$ minimum is about 200 m.

The second minimum (Fig. 6b), at 2.7 km can not be interpreted with confidence because there are no other physical clues to corroborate the measurement. Moreover spatial continuity can not be used because it is not possible to obtain two independent radials of data from the available time samples. It could be that the drop breakup and the associated drop oscillations contributed to the decrease in $\rho_{hv}(0)$ at 2.7 km.

A residual bias contributed by the aircraft motion was obtained from the stationary ground echoes as 18.5 m S-l and this bias was removed from the measured Doppler velocity. The results are presented in Fig. 6c where upward velocities are denoted as positive. The increase in fall velocity due to melting and subsequent decrease that might be due to drop break up are clearly evident in the velocity profile. The Doppler velocity has been unambiguously recovered from the time series data after compensating for the differential phase shift, $\phi_{DP}$, using an algorithm proposed in [11].

The Doppler spectrum width Fig. 6d shows two distinct and narrow peaks; one greater than 9 m S-l just above the peak in the Z profile and the other of 6.5 m S-l at about 2.7 km. Precisely at these heights the $|\rho_{hv}(0)|$ attains local minima. This is expected because contribution by wobbling of hydrometers is common to both increase of $\sigma_v$ and decrease of $|\rho_{hv}(0)|$ and the effect is much stronger at 2.2 cm wavelength than at 10 cm. Thus the spectrum width at vertical incidence and short wavelength might have a diagnostic value for microphysical interpretation.

It is necessary to carry out detailed analysis on longer data records from airborne platforms over known precipitation systems, to sharpen the above speculations in a more conclusive way. Such an opportunity arose on Feb9, 1993 during the TOGA COARE experiment.

The data from Feb9, 1993 were recorded in Cyclone Oliver off NE Australia in the Coral sea. The rainfall was generally stratiform with some embedded convection. The PRF was 4.8 kHz and the aircraft was making a spiraling accent with a roll of 10°. The radar antenna was scanning across the flight track, and a radial 'of time series data was collected at 10° off nadir (Fig. 2). Because the scanning is accomplished by rotating the feed, at 20° from the aircraft axis the polarizations are rotated clockwise by 20° (i.e. the drops are canted) as depicted in Fig. 2.

The aircraft was at the top of the melting layer whose peak is seen at 4.6 km in Fig. 7a. In this and subsequent figureswe have plotted the variables over a height interval of 4 to 5 km because there were no significant polarimetric features at lower heights. The top data point, at4.7 km, is the first available and it is 750 m away from the aircraft. A distinct signature in the correlation coefficient is evident in Fig 7a. $|\rho_{hv}(0)|$ was obtained from (A.4); other

estimators (Appendix) produced similar values because the signal to noise ratios are high and the spectrum is narrow. Below the melting layer the velocity (Fig. 7b) is generally negatively correlated with the reflectivity which is expected for precipitation in stagnant air." It is unlikely that the air was free of up/down drafts and furthermore there are contributions from horizontal air motions; thus it is not possible to relate the Doppler velocities to the terminal fall speed of particles. The spectrum width (Fig. 7c) has a maximum at the bottom of the melting layer similar to observations in Fig. 4d.

Surprisingly the differential reflectivity (Fig. 7d) and phase (Fig. 7d) have a distinct signatures even though the angle of observation is 10° off nadir. Both $Z_{DR}$ and $\phi_{DP}$ have local extrema at the bottom of the melting layer. Nevertheless the location of the $\phi_{DP}$ minimum is about 100 m higher than the location of the $Z_{DR}$ maximum. We attribute the -2.5° change of $\phi_{DP}$ to backscatter differential phase $\delta$. Note that the differential phase of the radar system is -46.5°.

To explain the signature in $Z_{DR}$, and $\delta$ we refer to Fig. 3 and the paper by Zrnic et al. [7] who observed change in size of aggregates from about 7 mm in the upper part of the melting layer to over 10 mm at the bottom. It might be that the precipitation at the minimum of $\delta$ consists of aggregates 10 to 12 mm in size mixed with small drops and other ice forms. Negative $\delta$ of about 2° can be produced by this size range if the axis ratio is 0.3 (Fig. 3), and larger negative values are expected for smaller axis ratios. Slightly below this minimum larger aggregates are likely present and if these are in the range of 12 to 14 mm [7] the backscatter differential phase will be smaller (Fig. 3). But, the differential reflectivity in this 12 to 14 mm size interval continues to grow (Fig. 3), thus we expect its maximum to be at a lower height than the minimum of

δ.

## 5. SUMMARY

Theoretical and experimental evidence points toward several possible uses of the correlation coefficient between horizontally and vertically polarized echoes that is obtainable with vertically or nadir looking radars. $|\rho_{hv}(0)|$ provides sharp signatures of the bright band bottom. Precipitation below the melting level consists of a varying mixture of hydrometers with diverse shape, size, and thermodynamic phase. The presence of such mixtures can result in an observable decrease of $|\rho_{hv}(0)|$ at vertical incidence. The largest contribution to decorrelation seems to come from wet aggregates; this is substantiated by consideration of two simple models. One is randomly oriented wet prolate spheroids and the other is distorted spheres. Prelates with axis ratios of3 or distorted spheres with rms roughness equal to 15% of the diameter decrease the correlation to 0.8 at S-band. At Ku-band, the correlation decrease is a function of size and it is largest for 5 mm diameters.

Polarimetric data obtained with a 10 cm wavelength ground-based radar and a 2 cm airborne radar were examined. Principal conclusions about the melting layer are drawn from several ground based observations. The airbornd systme is a new instrumetn and two preilimary observations were analyzed. Conclusions bassed on the airborne data are in agreement with those drawn from the ground-based observations. The vertical extent of the $|\rho_{hv}(0)|$ minima is a few hundred meters and in one case was less than the resolvable length of the measurement (150 m for the 10 cm wavelength radar). Precipitation immediately below the

minima is rain and that is deduced from distinct Doppler shift caused by the terminal velocities of drops. Col ocated with the Doppler shift is an abrupt change in the spectrum width that reflects the spread of terminal velocities. Because these two changes coincide with the $|\rho_{hv}(0)|$ minima, it is concluded that large irregular aggregates, their collapse into drops, and breakup of big drops are the most likely reasons for the observed signatures.

Airborne radar data also exhibit $|\rho_{hv}(0)|$ signatures that are useful in identifying the melting layer and to some extent, the type ofhydrometeors that are likely present. With the 50 mresolution of the airborne radar data, it was observed that the vertical extent of $|\rho_{hv}(0)|$ minimum is confined to about 100 m. In one case the decrease in $|\rho_{hv}(0)|$ to about 0.6 at 13.8 GHz inconsiderably larger than that observed with the ground based radar at 2.88 GHz. But in the other case the decrease to 0.9 is comparable, This might be due to presence of larger sizes (10 to 14 mm in diameter) for which the theory predicts a smaller decrease of correlation.

Indication that such large sizes were present are also suggested by the " -2.5° backscatter differential phase and 0.5 dB differential reflectivity. Measurements of these parameters were madeat IO" off nadir and we attribute the signatures to Mie scattering effects. Thus polarimetric measurements with high frequency radars might be suited for surprisingly small (10°) off nadir angles.

Aircraft motion contributes to increase the Doppler spectrum width. Inone case the width was 9 m S-l and the pulse pair type of estimator for $\rho_{hv}(0)$ was inadequate for analyzing the data because the correlation at lag 2 was very small. Four other estimators that use interpolation either in the frequency or in the time domain were tested to recover $|\rho_{hv}(0)|$ signatures from the airborne radar data. Interpolation using Fourier transform recovers the correlation

coefficient of data with the large spectrum width.

A desire to locate the bottom of the bright band is not a prime motivating factor behind this research. There are simpler techniques to locate the bright band. For example, the transition between ice and liquid precipitation can be found by observing the change in the mean Doppler velocity or spectrum width. But the correlation coefficient might provide discriminating signatures of hydrometers, which is not possible with use of the spectral moments. Indications are that different ice crystals should cause distinct decrease in the correlation coefficient, but there are no in situ measurements to confirm this hypothesis. Independent verification is crucially important for data interpretation and confidence in the polarimetric variables.

Estimation of the correlation coefficient is fairly simple; furthermore $|\rho_{hv}(0)|$ has an advantage over the linear depolarization ratio because it involves measurement of two strong signals as opposed to a strong and weak signals needed for the linear depolarization ratio.

## 6. ACKNOWLEDGMENTS

A. Zahrai has contributed substantially to the upgrade of the Cimarron radar facility. M. Schmidt has made numerous design changes and modifications of various hardware; he is also maintaining the facility with the help of G. Anderson and R. Wahkinney. Collaboration with K. Aydin and V. N. Bringi lead to insights in the interpretation of polarimetric data. Joan O'Banon generated two figures and Brent Gordon provided one figure for this paper. Part of the work was performed by the Jet Propulsion Laboratory, California Institute of Technology, under contract with NASA. Research at NSSL was supported in part by the NASA order number S-64075-E.

## APPENDIX

Examples of $|\rho_{hv}(0)|$ computed by various algorithms on the data setof"May 25, 1992 are presented here.

A procedure suggested by Balakrishnan and Zrnic [5] is based on two assumptions. First, some a priori model for the power spectral shape such as Gaussian is needed [3]. Second, the correlation at lag $(2\,m + 1)T_s$ (where $T_s$ is the pulse repetition time) is assumed to contain independent contributions from Doppler spectral broadening and $\rho_{hv}(0)$, so that it can be expressed as a product $\rho(2\,m + 1) \cdot \rho_{hv}(0)$, [11]. The correlation due to Doppler spread at lag $2T_s$ is

$$p(2) = \frac{\sum (H_{2i} H^*_{2i+2} + V_{2i+1} V^*_{2i+3})}{(M+1)\,(\hat{P}_h + \hat{P}_v)} \qquad (A1)$$

where $H_{2i}$ and $V_{2i+1}$ are two successive complex echo samples, $P_h$ and $P_v$ are the mean sample powers at H and V polarizations, M is the number of H or V sample pairs, and $\hat{}$ denotes estimates. An estimate of $\rho_{hv}(1)$ is obtained as

$$|\hat{\rho}_{hv}(1)| = \frac{|\hat{R}_a| + |\hat{R}_b|}{2\sqrt{\hat{P}_h \hat{P}_v}}, \qquad (A.2)$$

where $R_a$ is the autocorrelation between successive H and V polarized echoes and $R_b$ is the autocorrelation between V and H polarized echoes.

The correlation coefficient is. computed directly from Eqs. (A. 1) and (A.2) as

$$\hat{\rho}_{hv}(0) = |\hat{\rho}_{hv}(1) / \hat{\rho}(1)| = |\hat{\rho}_{hv}(1)| / |\hat{\rho}(2)|^{1/4}, \qquad (A.3)$$

because the assumption of Gaussian spectral shape permits equating $|\rho(1)|$ to $|\rho(2)|^{0.25}$.

The powers $P_h$ and $P_v$ in (Al) and (A.2) contain both signal and noise, therefore a correction needs to be incorporated to eliminate the noise bias. The following multiplicative correction of either prevents generation of negative powers:

$$P_c = \frac{P(S/N)}{(S/N+1)}, \qquad (A.4)$$

where PC stands for corrected power, S is the signal power, and N is the white noise power.

Equation A.3 without noise correction (i.e. S/N >>1) is used in the programmable signal processor on the Cimarron radar, but the correction is applied to the recorded $|\rho_{hv}(0)|$ later. Although the estimate of the receiver noise is very accurate, other contributions such as quantization noise and external interferences can still bias the correlation coefficient. We made an attempt to estimate the noise in the spectra from the airborne radar but were often not successful because the spectra are very broad.

The power density (Doppler) spectrum of the horizontally polarized sequence taken at 4.155 km above ground level (May 25, 1992) is shown in Fig. Al. It is apparent that the spectral shape is not Gaussian and furthermore the spectrum is broad so that the correlation at lag 2 is small! These are the reasons that the estimator (A.3) is not reliable and has produced values larger than 1 at two heights (Fig A.2a).

There are several other techniques that can be used to calculate the

$|\rho_{hv}(0)|$ from an alternating sequence of H and V time series data. We present results of more robust computations in the following paragraphs.

$\rho_{hv}(0)$ can be estimated from the correlation between Hand Vpower spectra. If H(f) and V(f) denote the complex Fourier Transform of H(t) and V(t), $\rho_{hv}(0)$ . can be written as

$$\rho_{hv}(0) = \frac{cov(H(f), V(f))}{\sqrt{Var(H(f))Var(V(f))}} \qquad (A.5)$$

This estimate of $|\rho_{hv}(0)|$ for the May 25, 1992 data is presented in Fig. A.2b. Note that the estimator does not interpolate the H,V samples and hence contains contributions from the Doppler spectral broadening.

The H and V can be interpolated so that a coincident set of H and V time samples is obtained and the complex correlation coefficient can be calculated in the conventional way. The interpolation of the H and V time series data can be done by first computing the Fourier transform of the data, padding the transform with equal number of zeros to double the Nyquist frequency and then taking the inverse Fourier transform. $|\rho_{hv}(0)|$ computed using this technique is shown in Fig. 6b of this paper. It can be shown that identical results are obtained if the spectral coefficients of H and V series are compensated for the phase shift $\omega_i T$ (where $\omega_i$ is the Doppler frequency if the i th spectral coefficient) caused by the time delay T between the measurement of H and V samples.

The $|\rho_{hv}(0)|$ (not shown) obtained using a simple linear interpolation of the H and V complex samples in the time domain has the lowest values of all considered estimates.

REFERENCES

[1] Kumagai, H., R. Meneghini and T. Kozu, 1993: Preliminary results from multiparameter airborne rain radar measurement in the Western Pacific. *J. Appl. Met., 32, 431-440.*

*[2]* Zrnic, D. S., R. Raghavan, and V. Chandrasekar, 1993b: Observations of co-polar correlation coefficient through a bright band at vertical incidence. *J. Appl. Meteorol.*, 32,

[3] Doviak, R. J., and D. S. Zrnić, 1993: Doppler Radar and Weather Observations, Academic Press, Orlando, FL, p 562.

[4] Zahrai A., and D. S. Zrnic, 1992: A 10 cm wavelength polarimetric radar of the NOAA's National Severe Storms Laboratory. (accepted by the *J. Atmos. Ocean. Tech.)*

*[5]* Balakrishnan, N., and D. S. Zrnic, 1990: Use of polarization to characterize precipitation and discriminate large hail. *J. Atmos. Sci., 47, 1525-1540.*

*[6]* Sachidananda, "M., and D, S. Zrnić, 1985: $Z_{DR}$ measurement considerations for a fast scan capability radar. *Radio Sci., 20, 907-922.*

*[7]* Zrnic, D. S., N. Balakrishnan, C. L. Ziegler, V. N. Bringi, K. Aydin, andT. Matejka, 1993: Polarimetric signatures in the stratiform region of a mesoscale convective system. *J. Appl. Meteorol., 32, 678-693.*

*[8]* Illingworth, A. J., and 1, J. Caylor, 1991: Co-polar measurement of precipitation. *Preprints, 25th Conference on Radar Meteorology*, Paris, France, AMS, 650-653.

[9] Waterman, P. C., 1969: Scattering by dielectric obstacles. *Alta Freq., 38, 348-352.*

*[10]* Battan, L. J., 1973: Radar Observation of the Atmosphere. Univ. of

Chicago Press, Chicago, Ill, p 324.

[11] Sachidananda, M., and D. S. Zrnic', 1989: Efficient processing of alternately polarized radar signals. *J. Atmos. Oceanic Technol.*, *6, 173-181.*

FIGURES

Fig. 1 Correlation coefficient for randomly oriented prolate spheroids, versus diameter. The axis ratios, a/b, are indicated. The dielectric constant is that of water ($\epsilon_r$=29.52 + j37.76); the frequency is 13.8 GHz.

Fig. 2 Data acquisition geometry and polarization coordinates for the experiment on Feb 9,1993.

Fig. 3 Differential reflectivity defined as a difference between reflectivity factors (in dBZ) for horizontal and vertical polarization and backscatter differential phase defined as the difference between backscatter phase at horizontal and vertical polarization for oblate water spheroids. The frequency is 13.8 GHz, the dashed curve is for axis ratio of 0.4 and the solid curve is for axis ratio of 0.3. The incidence angle is 10° and the fields are rotated. by 20° clockwise (i.e., the hydrometer is canted by 20°).

Fig. 4 a) Magnitude of the correlation coefficient at vertical incidence obtained with the Cimarron radar, b) the reflectivity factor, c) the Doppler velocity and d) the spectrum width. Data are averages from 50 consecutive radials over a time of 16 s, the transient of the polarization switch lasts 7 $\mu$s and therefore there are no valid data below 1 km. The date is June 5 1992 and time is 14:33 UT; on this day the zero degree isotherm in the environment was at 3.6 km. e) Detail of the significant changes in $|\rho_{hv}(0)|$, Z, and v through the melting layer.

Fig. 5 Time height cross section of the correlation coefficient for June 5, 1992. The graph contains 1000 radials collected during a 390 s time interval.

Fig. 6 Vertical profiles of a) reflectivity factor, b) correlation coefficient,

c) velocity, and d) spectrum width, from the airborne radar. The date is May 25, 1992 and the data were obtained with the airborne radar.

Fig. 7 Vertical profiles ofa) reflectivity factor and correlation coefficient, b) velocity (a 5.3 m S-l component due to aircraft motion was removed), c) spectrum width, and d) differential reflectivity and differential phase, from the airborne radar. 400 time series samples were used for the estimates. The date is Feb 9, 1993 and the data were obtained with the airborne radar.

Fig. A.1 Power spectra of the horizontally polarized sequence; the vertically polarized sequence has similar power spectra, The data are from 4.1 km above ground on May 25, 1992.

Fig. A.2 Vertical profiles of $|\rho_{hv}(0)|$ computed by a) pulse pair type algorithm eq (A.3), and b) correlation of power spectra, This data was acquired by the airborne radar on May 25, 1992.

TABLE 1

Cimarron Radar Parameters

| | |
|---|---|
| Frequency | 2735 MHz |
| Peak power | 500. kW |
| Beam width | 0.9 deg |
| Maximum side lobe level | -22 dB |
| Antenna gain | 46 dB |
| Pulse width | 1 μs |
| Receiver noise level | -110 dBm |
| Matched filter bandwidth (6 dB) | 0.85 MHz |
| System losses | 11.7 dB |
| Cross polar isolation | 20 dB |

TABLE 2

ARMAR Parameters

| | |
|---|---|
| Frequency | 13.8 GHz |
| Peak power | 200 W |
| Beam width | 3.8 deg |
| Polarization | H(H)V(V) |
| Maximum side lobe level | -32 dB |
| Antenna gain | 34 dB |
| Pulse width | 5 - 45 μs |
| Receiver noise level | -104 dBm |
| Bandwidth | 4 MHz |
| Pulse Repetition Frequency (PRF) | 1 - 8 kHz |
| Range resolution (3 dB) | 55 m |
| Number of range gates | 512 |
| Flight altitude | 12 km |
| Aircraft speed | 240 m S-l |

D204283

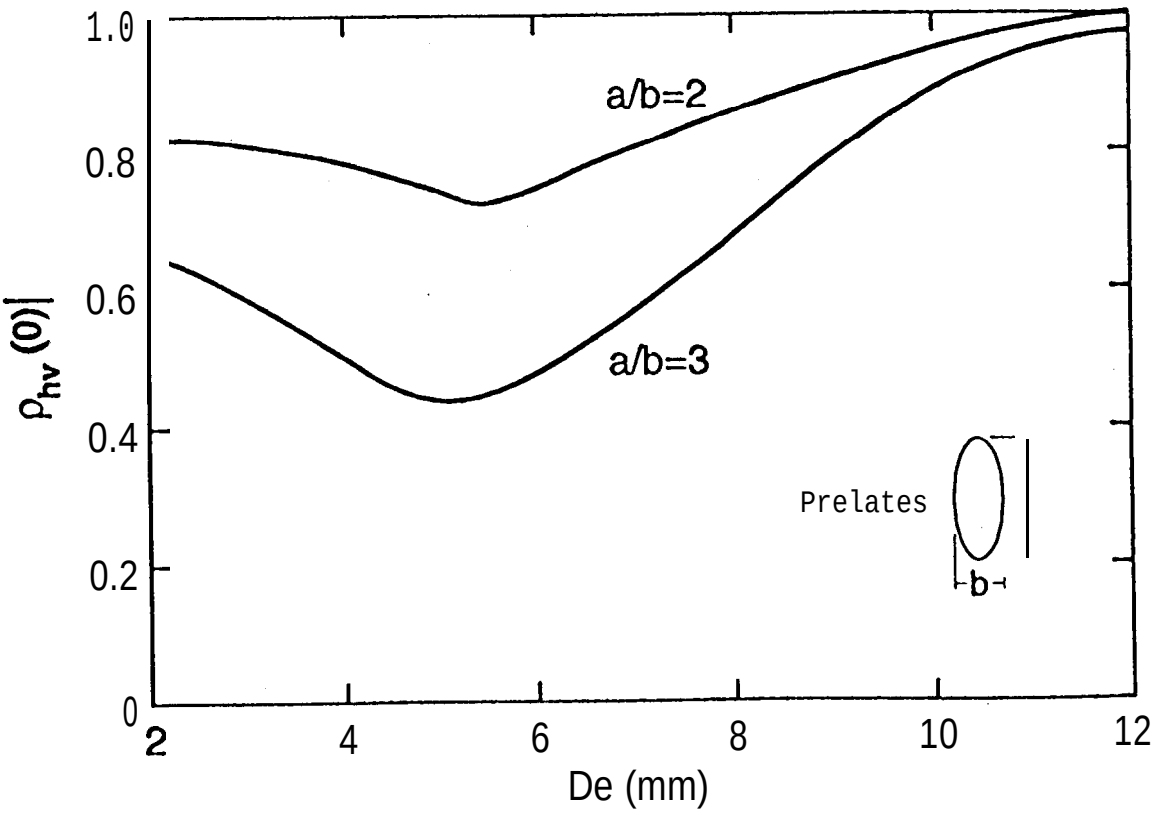

D203303

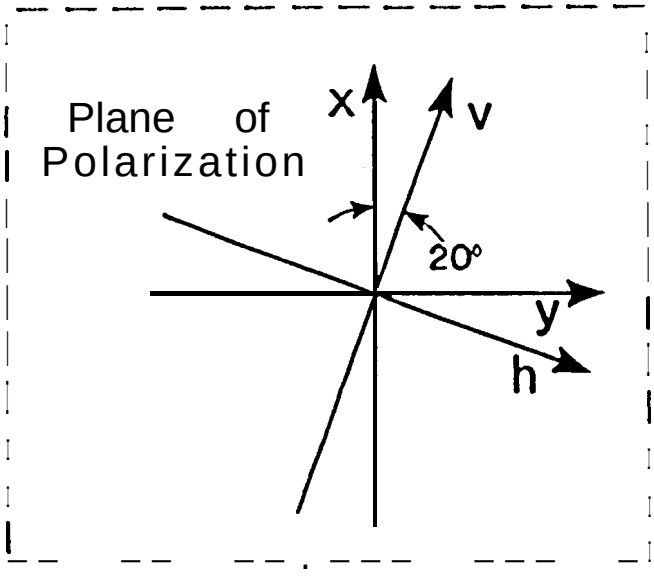


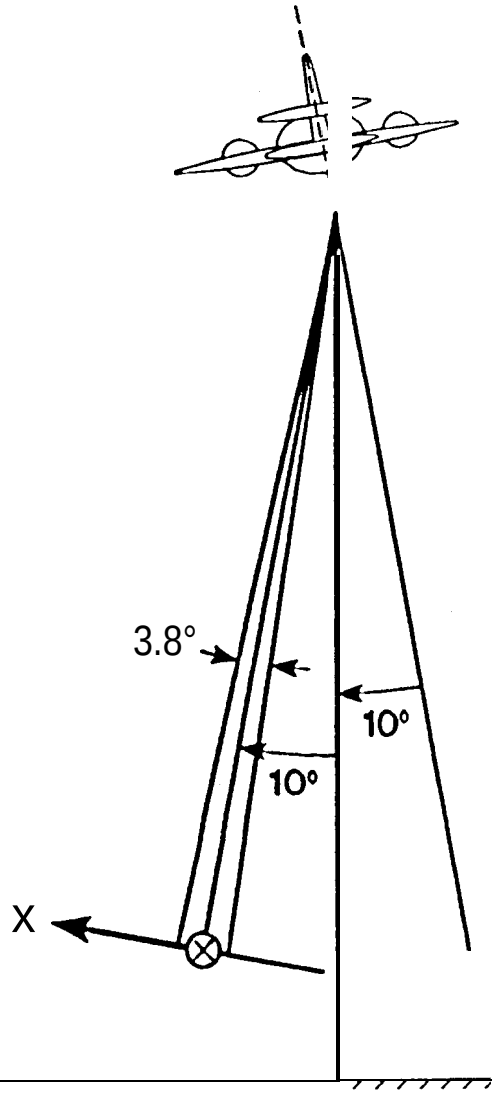

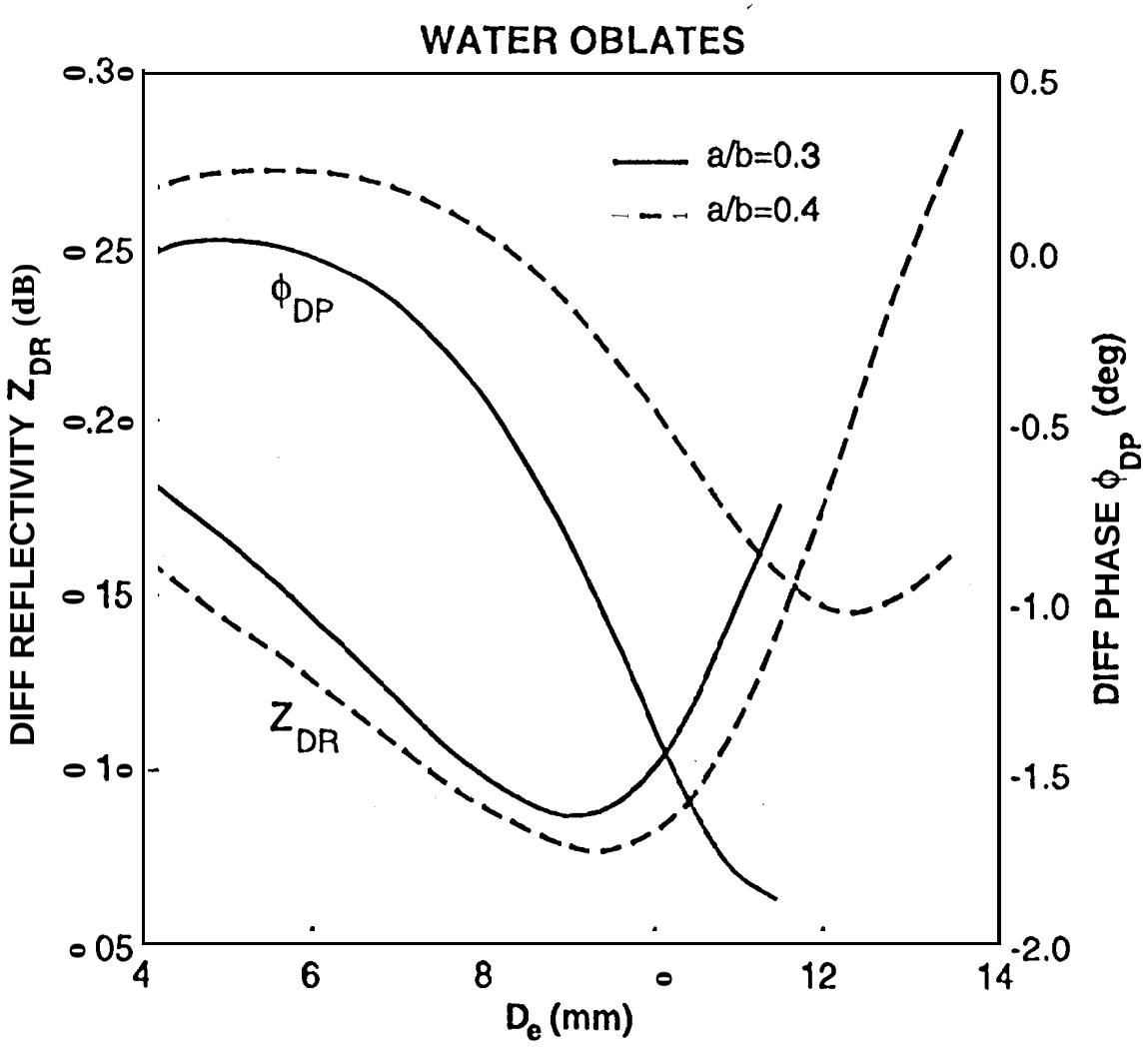
WATER OBLATES
a/b=0.3
a/b=0.4
$\phi_{DP}$
$Z_{DR}$
DIFF REFLECTIVITY $Z_{DR}$ (dB)
DIFF PHASE $\phi_{DP}$ (deg)
$D_e$ (mm)
0.3
0.25
0.2
0.15
0.1
0.05
0.5
0.0
-0.5
-1.0
-1.5
-2.0
4
6
8
12
14

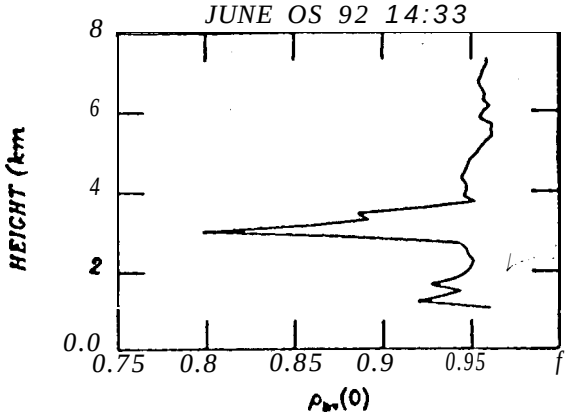
JUNE OS 92 14:33
8
6
4
2
0.0
HEIGHT (km
0.75
0.8
0.85
0.9
0.95
f
$\rho_{bv}(0)$

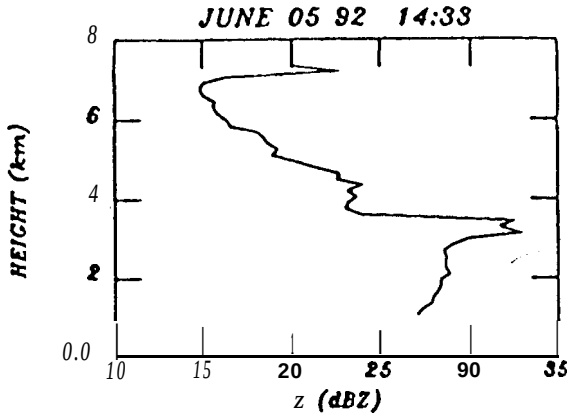
JUNE 05 92 14:33
8
6
4
2
0.0
HEIGHT (km)
10
15
20
25
90
35
z (dBZ)

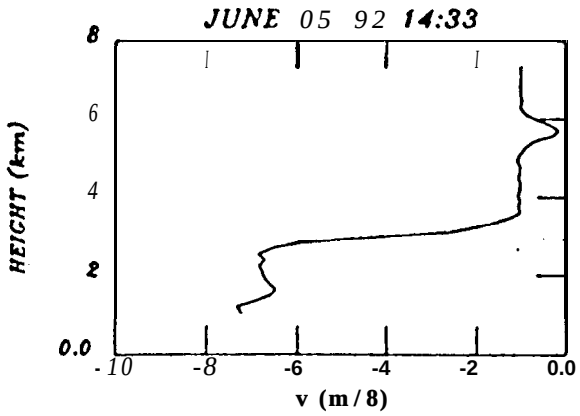


4c

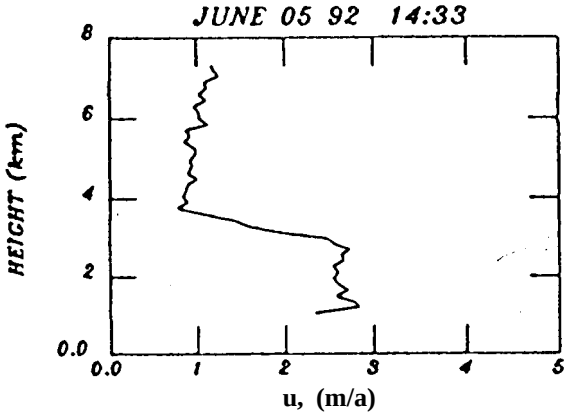


4d

DZ03293

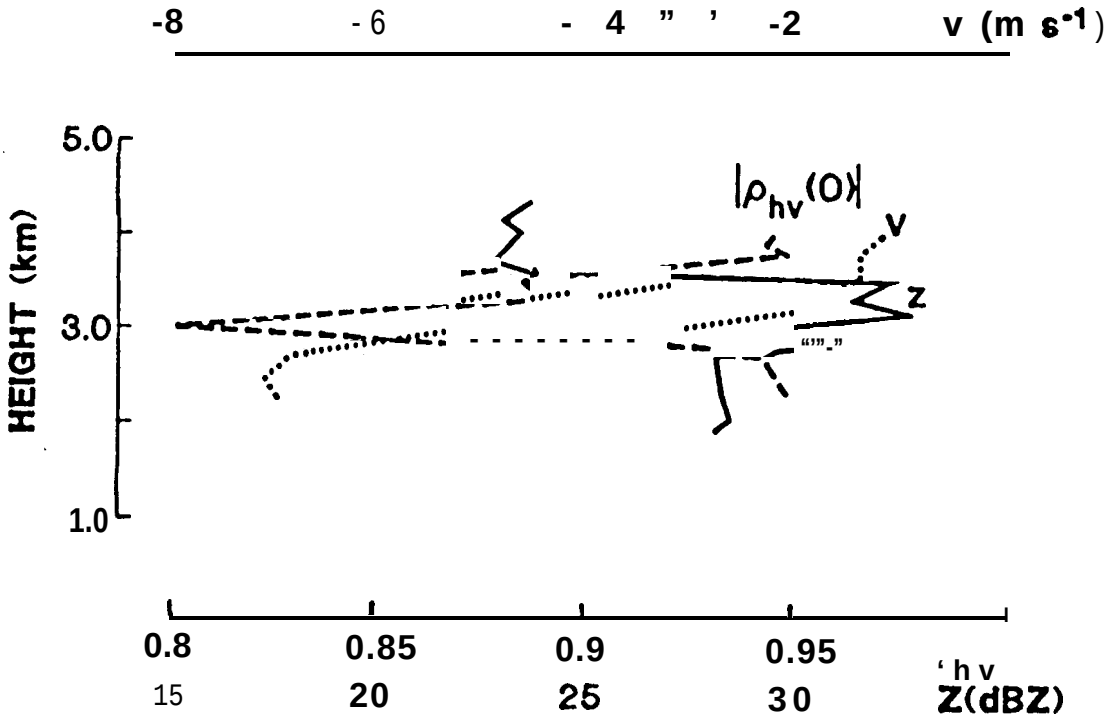
-8
- 6
- 4
-2
v (m s-1)
5.0
3.0
1.0
HEIGHT (km)
|ρhv(0)|
v
Z
0.8
0.85
0.9
0.95
15
20
25
30
'hv
Z(dBZ)

4e

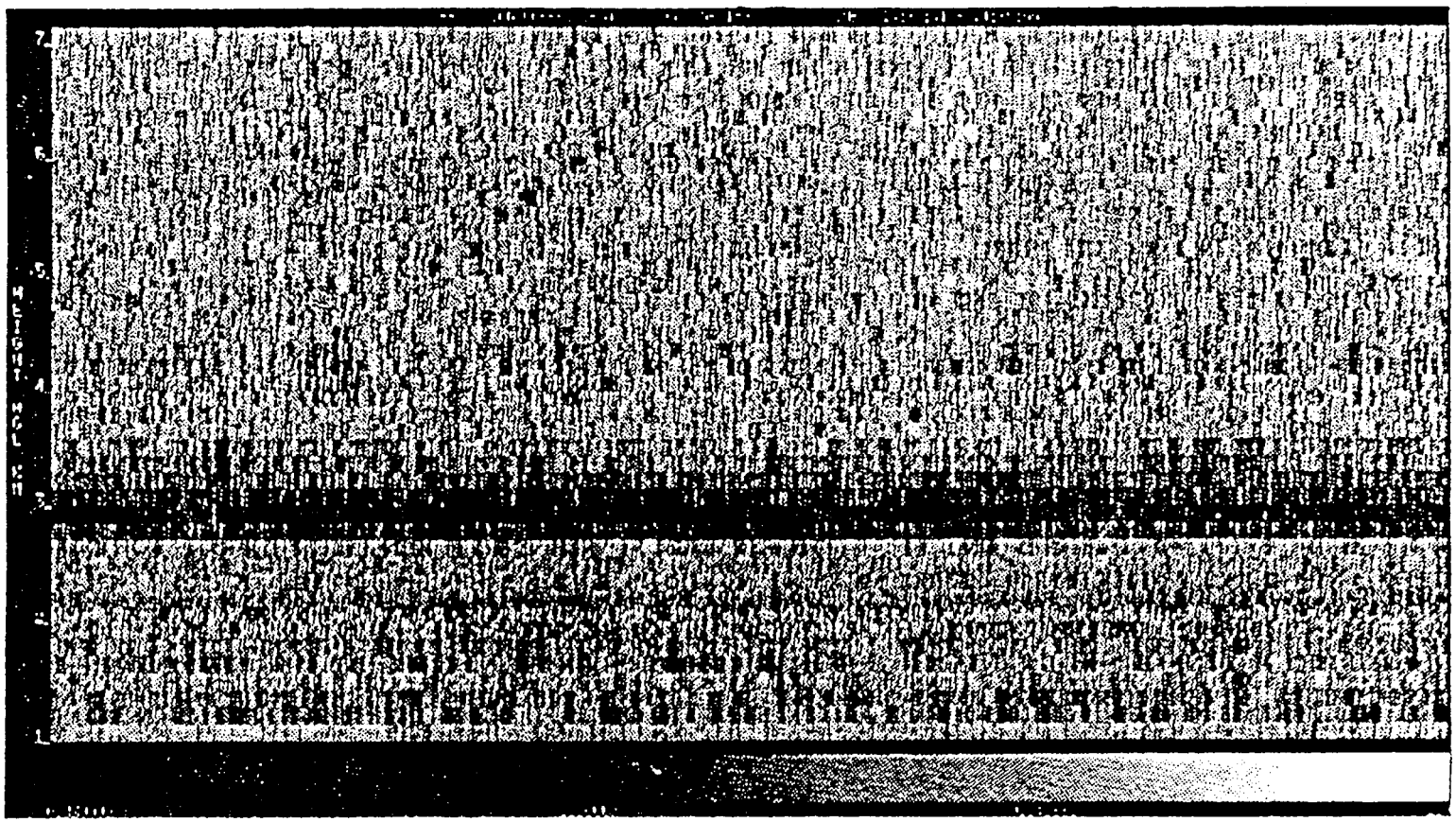

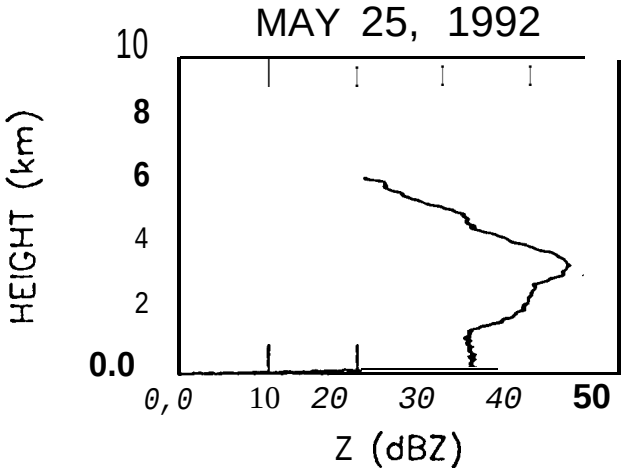


6a

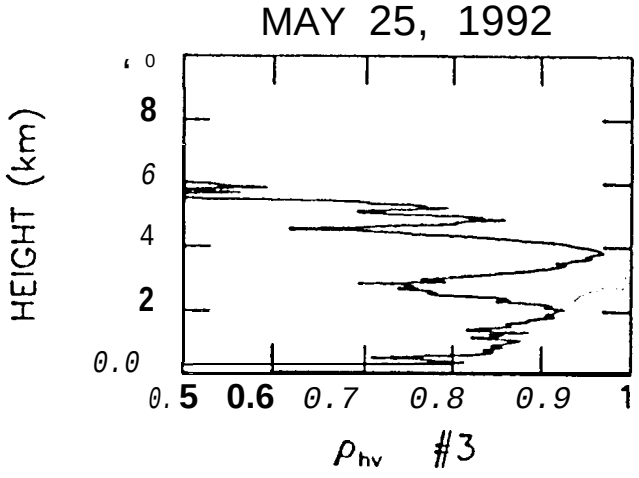




Interpolation reading Rees

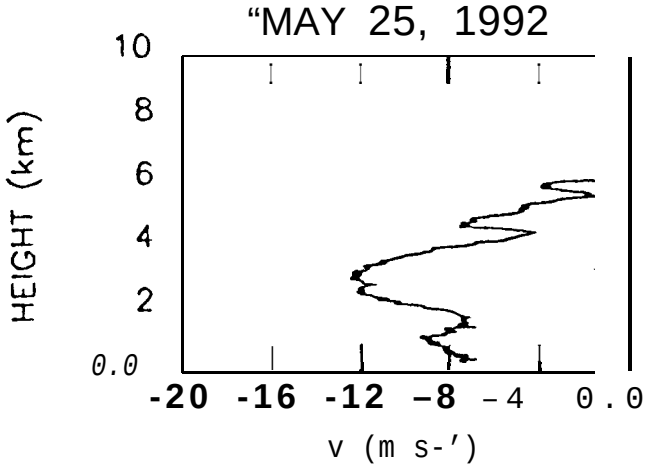


6C

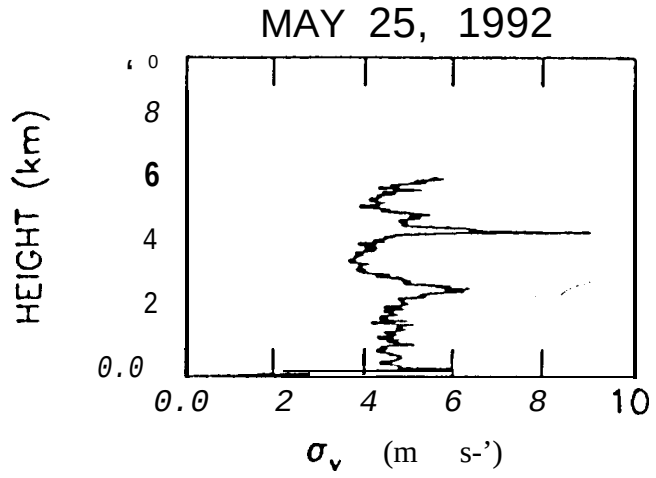


6d

DZ080430

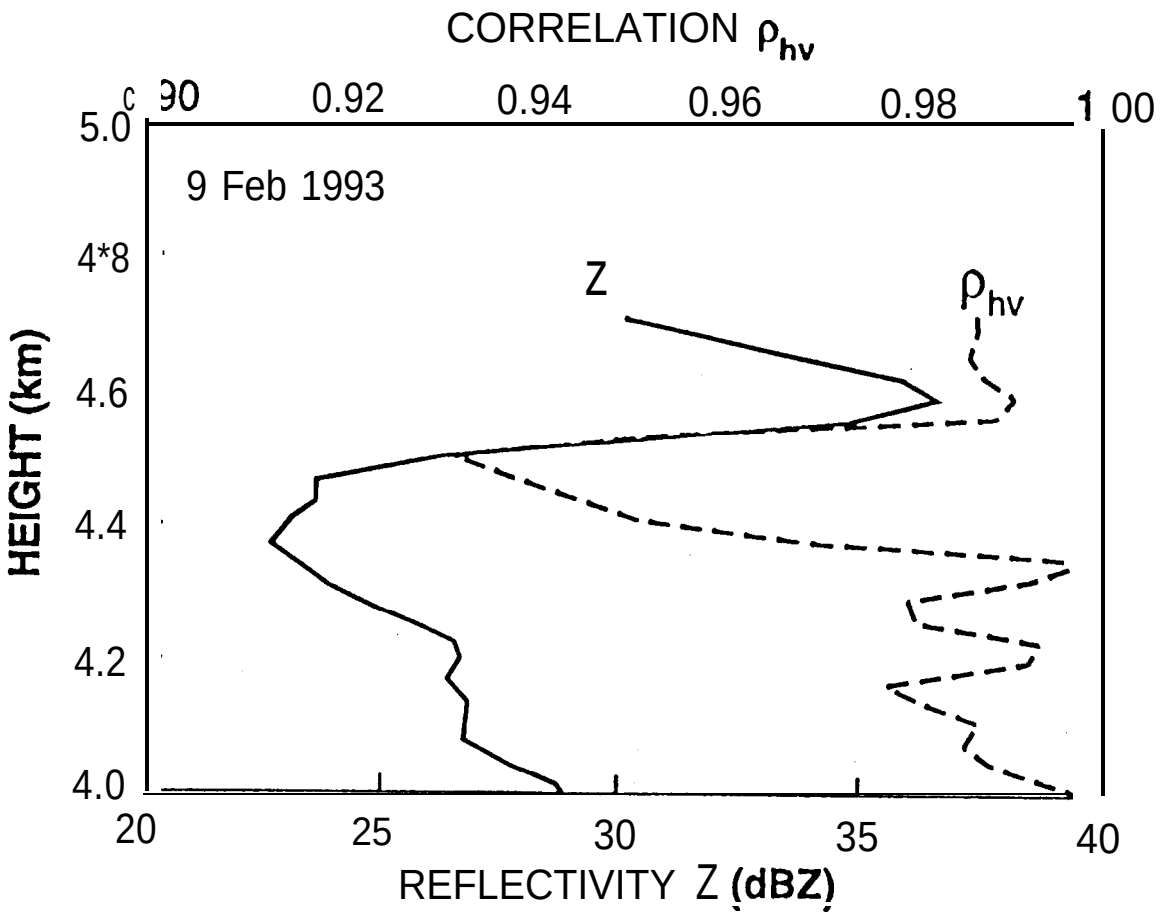
CORRELATION $\rho_{hv}$
c 90
0.92
0.94
0.96
0.98
1 00
5.0
9 Feb 1993
4*8
Z
$\rho_{hv}$
HEIGHT (km)
4.6
4.4
4.2
4.0
20
25
30
35
40
REFLECTIVITY Z (dBZ)

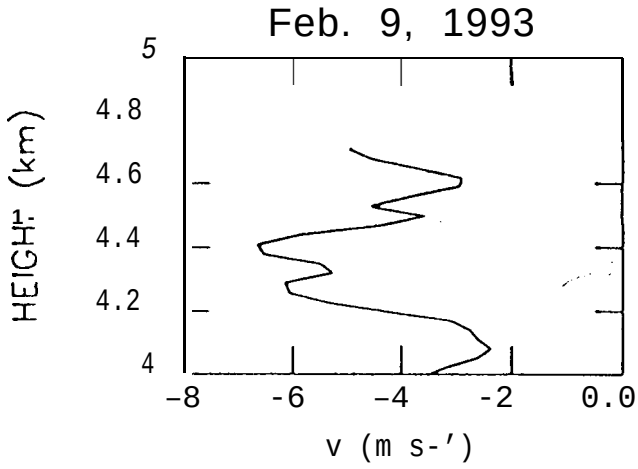
Feb. 9, 1993
HEIGHT (km)
5
4.8
4.6
4.4
4.2
4
−8
-6
−4
-2
0.0
v (m s-')

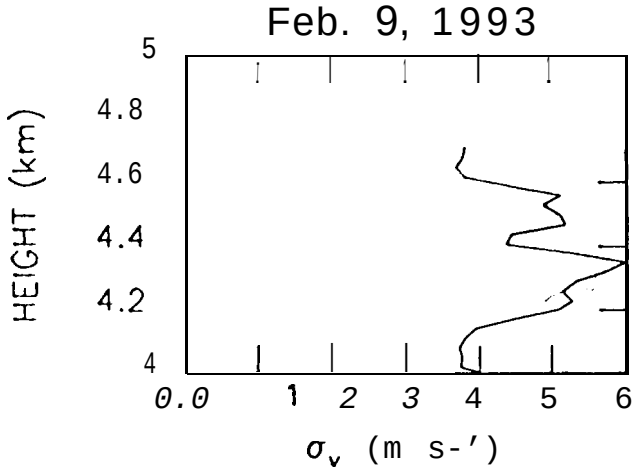


7c

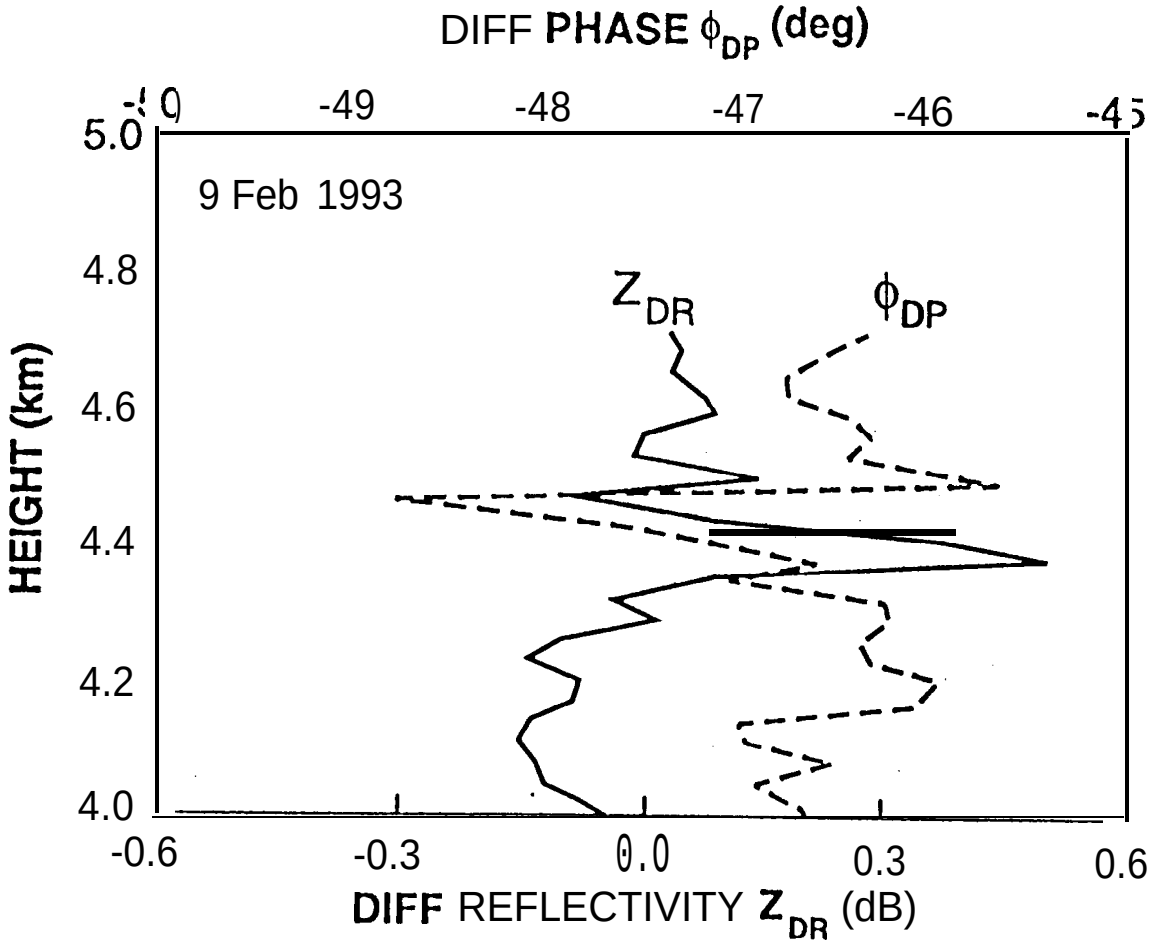
DIFF PHASE $\phi_{DP}$ (deg)
-50
-49
-48
-47
-46
-45
5.0
4.8
4.6
4.4
4.2
4.0
9 Feb 1993
$Z_{DR}$
$\phi_{DP}$
HEIGHT (km)
-0.6
-0.3
0.0
0.3
0.6
DIFF REFLECTIVITY $Z_{DR}$ (dB)

7d

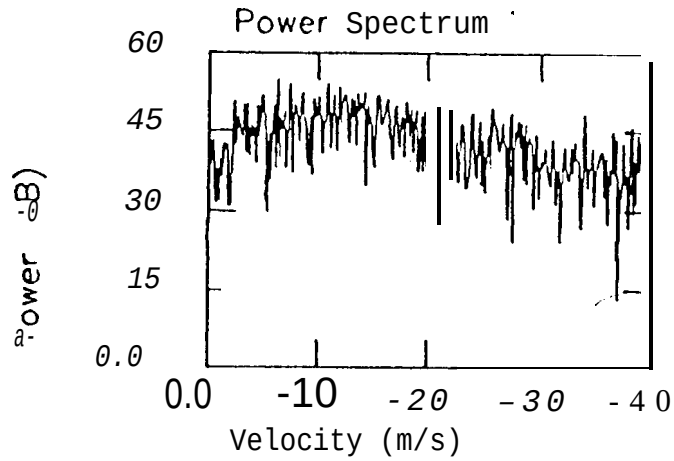
Power Spectrum
60
45
30
15
0.0
Power (dB)
0.0
-10
-20
-30
-40
Velocity (m/s)

A-1

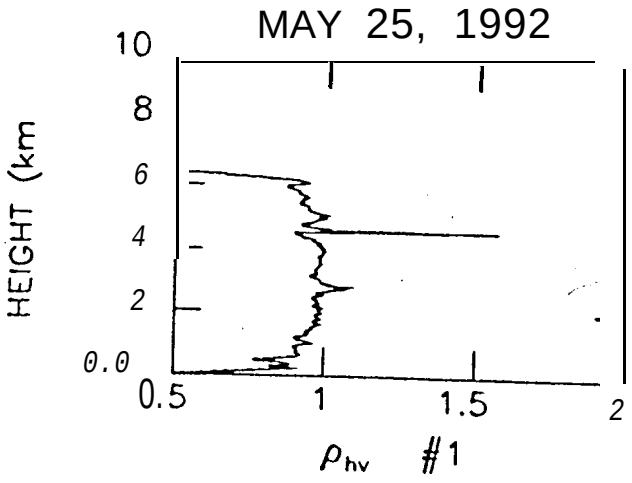


A.2a

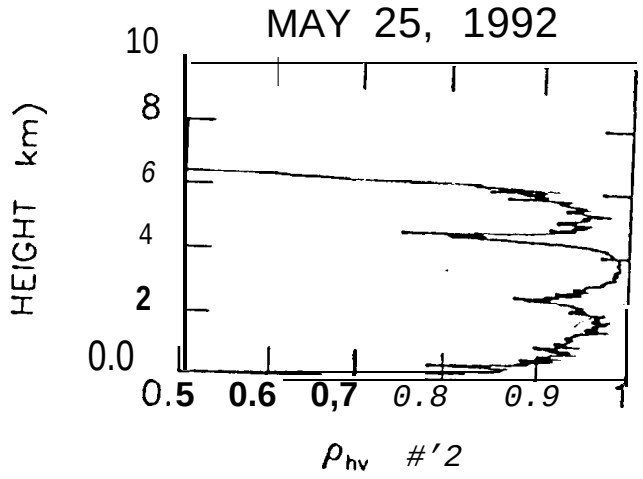


A.2b